# *Supporting Information*

# Rapid Joule heating synthesis of Ni doped into porous honeycomb $C_3N_4$ with greatly improved photocatalytic $H_2$ production

Zehui Zhao[1], Guangmin Ren[1], Zisheng Zhang[2], Xiangchao Meng[1] and Zizhen Li[1,2*]

[1]Key Laboratory of Marine Chemistry Theory and Technology, Ministry of Education, College of Chemistry and Chemical Engineering, Ocean University of China, Qingdao 266100, China

[2] Department of Chemical and Biological Engineering, Faculty of Engineering, University of Ottawa, Ottawa, Ontario, K1N6N5, Canada

*Corresponding author.

E-mail address: lizizhen@ouc.edu.cn

# S1. Experimental Section

## 1.1. Chemicals

Nickel nitrate hexahydrate ($Ni(NO_3)_2 \cdot 6H_2O$, AR) was purchased from Sinopharm Chemical Reagent Co., Ltd. (China) and used without further purification. Melamine ($C_3H_6N_6$, ≥99.0%) was ordered from Sinopharm Chemical Reagent Co., Ltd. (China) and used for preparing catalysts. Tetraethyl orthosilicate ($C_8H_{20}O_4Si$, >99%) was purchased from Macklin Biochemical Technology Co., Ltd (China). Ethanol absolute ($C_2H_6O$, AR) and ammonia solution ($NH_4OH$, AR) were ordered from Sinopharm Chemical Reagent Co., Ltd. (China). Nafion (5%) was purchased from Aladdin Ltd. (Shanghai, China). Ultrapure water used throughout all experiments was purified through an ACMATE system.

## 1.2. Materials synthesis

*Synthesis of $SiO_2$ nanospheres*: $SiO_2$ nanospheres were prepared according to the reported synthesis method.[1] Specifically, 55 mL of absolute ethanol, 15 mL of deionized water, 3 mL of tetraethyl orthosilicate and 4 mL of ammonia solution were added into a beaker and stirred for 5 h to obtain a milky white suspension. The powder sample was separated and washed. Then, the sample was vacuum dried at 80°C for 12 h to obtain solid powder $SiO_2$.

*Synthesis of honeycomb $C_3N_4$ (HCN)*: HCN was prepared by using a hard template approach. Firstly, 5 g of melamine and 2.4 g of $SiO_2$ hard template were uniformly mixed and then put into a crucible. Subsequently, the ceramic crucible was covered with a layer of tin foil. The mixed precursors were heated to 550°C in a muffle furnace

(CHEM$^N$, BFC-1200-7.2L) at a heating rate of 10°C/min and kept under air atmosphere for 2 h. Melamine underwent pyrolysis and thermal polymerization during heating to generate honeycomb porous $C_3N_4$, while the product was filled into the voids of the $SiO_2$ template. The obtained $C_3N_4/SiO_2$ was then treated with 100 mL of 2 mol/L NaOH for 12 h to etch away the $SiO_2$ nanosphere templates, and then the synthesized product was centrifuged and washed several times with distilled water and ethanol. Finally, the obtained product was dried at 60°C for 12 h and yellow $C_3N_4$ with a honeycomb structure was collected, which was labeled as HCN.

*Synthesis of $C_3N_4$ (BCN)*: For comparison, the silica template was not used and the $C_3N_4$ was obtained by replacing the mixed precursor with melamine powder in the above step. Typically, 10 g of melamine was put into a ceramic crucible covered with a layer of tin foil, and then heated to 550°C at a heating rate of 10°C/min in a muffle furnace for 4 h under an air atmosphere. Then, the yellow $C_3N_4$ was collected after cooling down to room temperature, which was labeled as BCN.

*Synthesis of honeycomb $C_3N_4$-$V_N$ (HCN-$V_N$)*: Firstly, HCN was placed in a molybdenum boat and put into the Joule heating equipment (In-situ High-tech, CIS-JH3.2), then evacuated and passed into Ar gas. Next, HCN-$V_N$ was synthesized by the rapid Joule heating treatment under an argon atmosphere. A high pulse voltage of 30 V was applied instantaneously to the HCN, and a strong pulse current of 300 A caused the HCN to rapidly reach the specified temperature within 10 seconds to obtain HCN-$V_N$. The heating rate was shown in Fig. S1a.

*Synthesis of Ni/honeycomb $C_3N_4$-$V_N$ (Ni/HCN-$V_N$)*: Generally, 0.50 g of HCN and the

specified amount of $Ni(NO_3)_2 \cdot 6H_2O$ were dispersed in 10 mL of deionized water and impregnated under a constant temperature water bath at 60°C for 4 h to obtain a suspension. The suspension was then separated by centrifugation and dried overnight in a vacuum drying oven at 80°C. The resulting product was named $Ni_x/C_3N_4$ (x = 1.0, 1.5, 2.0, 2.5, 3.0), where x represented the percentage of the actual mass of nickel in the composite. For comparison, we also prepared $Fe_2/C_3N_4$, $Co_2/C_3N_4$, $Ni_2/C_3N_4$, $Cu_2/C_3N_4$ with a mass fraction of 2.0 using $Fe(NO_3)_3 \cdot 9H_2O$, $Co(NO_3)_2 \cdot 6H_2O$ and $CuCl_2$ as precursors.

The above obtained samples were centrifuged and dried, and calcinated by the rapid Joule heating method with the same parameters as for the preparation of HCN-$V_N$, for different impregnation amounts, different loading metals, and different heating temperatures, where the best active sample was named Ni/HCN-$V_N$. The changed of the sample colors throughout the process were seen in Fig. S2.

*Synthesis of Ni/honeycomb $C_3N_4$-d-$V_N$ (Ni/HCN-d-$V_N$)*: In addition, to compare the conventional tube furnace method with the rapid Joule heating method, samples heated in a $Ni/C_3N_4$ tube furnace ($CHEM^N$ TFH-1200-60-440) were also prepared (denoted as Ni/HCN-d-$V_N$). The tube furnace heating rate was shown in Fig. S1b.

### 1.3. Characterizations

A powder X-ray diffractometer Bruker D8 Advance was used to determine X-ray diffraction (XRD) patterns, with a scanning angle in the range of 5-90° and a scanning speed of 10°/min. A TESCAN MIRA LMS equipped with EDS capabilities was used to obtain the scanning electron microscope (SEM), the samples were sprayed with gold

before scanning. A JEOL JEM-2100Plus Electron Microscope with a spherical aberration corrector was used to obtain the transmission electron microscopy (TEM), high-resolution TEM (HRTEM). A Bruker EMX plus-6/1 was used to obtain the electron paramagnetic resonance (EPR) spectra at 100 K. The XPS tests were determined on the Thermo Scientific Escalab 250Xi X-ray photo-electron spectrometer with Al Kα source. The in-situ XPS tests were also conducted on a Thermo Scientific Escalab 250Xi X-ray photo-electron spectrometer with Al Kα source, a 300 W Xe lamp was used as the light source in in-situ XPS tests. A Bruker TENSOR 27 FT-IR spectrophotometer over the range 4000-400 $cm^{-1}$ at 2 $cm^{-1}$ resolution was used to determine Fourier transform infrared (FT-IR) spectra. A UV-vis spectrophotometer (PUXI TU-1901) was used to determine the UV-Vis diffuse reflectance spectroscopy (DRS) and UV-Vis absorption spectrum, with a wavelength testing range of 200-800 nm, a high-speed scanning speed, and the measurement of absorption values. The Brunauer-Emmett-Teller (BET) were recorded using Micromeritics ASAP 2460 gas sorption analyzer at 77 K.

### 1.4. Photocatalytic $H_2$ production tests

Photocatalytic water splitting was carried out on an all-glass automatic online trace gas analysis system (Lab-solar-6A, Beijing Perfectlight). The light source was a 300 W Xe lamp (PLS-SXE300+, Perfectlight). The produced gas sample was analyzed using a gas chromatograph (7900, Techcomp, China). Before the test, the reactor needed to be vacuumed. As for the reaction, 50 mg of the sample was dispersed into 100 mL of 10 vol.% methanol aqueous solution through ultra-sonication. The mixture was

magnetically stirred. The distance between the lamp and the surface of the suspension was kept at 5 cm. To eliminate the thermal effect from Xe lamp, the temperature of the reactor was maintained at 25°C during the reaction by circulating water. The amount of produced $H_2$ was carried into GC for analysis by Argon gas. The concentration of produced $H_2$ was calibrated by peak area, and the concentration-peak area curve was calibrated using a standard hydrogen with a series of concentrations, the standard curve was y = 253.12x + 6329.47 (Fig. S3). In addition, the catalyst was centrifuged and used again in cycling experiments to test the hydrogen production rate to evaluate the reproducibility information of Ni/HCN-$V_N$. In addition, the apparent quantum efficiency (AQE) of Ni/HCN-$V_N$ was calculated using equations (1), (2) and (3). The average radiation intensities at 365 nm, 420 nm and 500 nm measured using an irradiance meter were 46.15 mW·cm$^{-2}$, 21.20 mW·cm$^{-2}$ and 16.56 mW·cm$^{-2}$.

$$AQE = \frac{2 \times the\ number\ of\ evolved\ hydrogen\ molecules}{the\ number\ of\ incident\ photons} \times 100\% \quad (1)$$

$$The\ number\ of\ evolved\ hydrogen\ molecules = N_A \times M \quad (2)$$

$$The\ number\ of\ incident\ photons = \frac{E\lambda}{hc} \quad (3)$$

where $N_A$ and M is the Avogadro's constant and the $H_2$ production rate (mol/s), respectively; E, λ, h and c represent the power of lamp source, wavelength, the Planck constant ($6.626\times10^{-34}$ Js) and the speed of light ($3.0\times10^{8}$ ms$^{-1}$), respectively.

### 1.5. Electrochemical tests

The electrochemical measurements were analyzed on a CHI 660E electrochemical workstation with a three-electrode system. The working electrode was an electrode holder with a conductive glass sheet coated with catalyst, the counter electrode was a

platinum electrode, and the reference electrode was a saturated Ag/AgCl electrode. A 300 W Xe light was used as the light source to measure the photocurrent response and electrochemical impedance spectra (EIS) of different samples in 0.5 M $Na_2SO_4$ aqueous solution. All working electrodes were obtained by the following method: 10 mg of catalyst and 20 μL of Nafion solution were ultrasonically dispersed in 200 μL of deionized water, and 50 μL of the solution was uniformly applied on 1 × 1 $cm^2$ FTO glass and dried at room temperature.

**1.6. Theoretical calculations**

DFT calculations were performed using the CASTEP module in the Materials Studio software. The exchange-correlation interactions are treated as Perdew - Burke - Ernzerhof (PBE) generalized functions in the generalized gradient approximation (GGA). The cutoff energy and the Monkhorst - Pack K-point are set to 500 eV and 3 × 3 × 1, respectively. During the structural optimization, the energy convergence criterion is 1.0 × 10 - 5eV/atom and the maximum displacement convergence criterion is 0.001 Å. A vacuum region of 20 Å is used to avoid interlayer interactions. The van der Waals forces (vdW) were corrected using the Grimme method (DFT-D2). The adsorption energy of the adsorption system was defined as Eads = E(Ni/HCN-$V_N$/H) - E(Ni/HCN-$V_N$) - E(H), where E(H) is the energy of the H, E(Ni/HCN-$V_N$/H) and E(Ni/HCN-$V_N$) are the total energy of the Ni/HCN-$V_N$ surface with and without the adsorbed H, respectively. Generally, the closer the hydrogen adsorption energy is to 0, the better the proton adsorption and hydrogen desorption behavior of the adsorption system.

To reveal the mechanism of HER on the surface of Ni/HCN-$V_N$ the first principle

calculations were performed, by using the projector augmented wave pseudopotentials and Perdew-Birke-Ernerhof exchange-correlation as implemented in Vienna *ab initio* simulation package (VASP).[2,3] The generalized gradient approximation method of Perdew-Burke-Ernzerhof (PBE) functional was used to describe the exchange-related interaction between electrons.[4] The van der Waals (vdW) correction with the Grimme approach (DFT-D2) was included in the interaction between single molecule/atoms and substrates6.[5] The convergence criteria for the total energy and the Hellmann-Feynman force were $10^{-5}$ eV and 0.02 eV, respectively.

## S2. Supporting figures

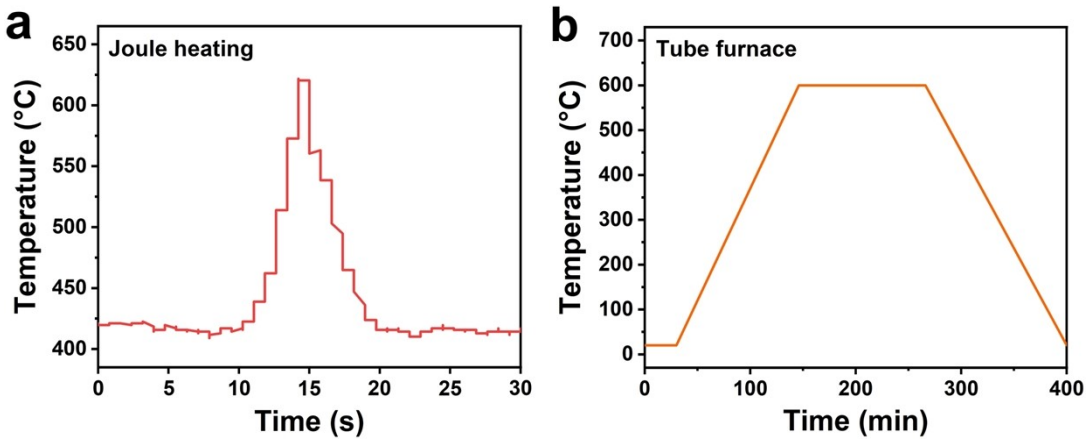


**Fig. S1.** Real heating curves of (a) Joule heating method and (b) tube furnace method.

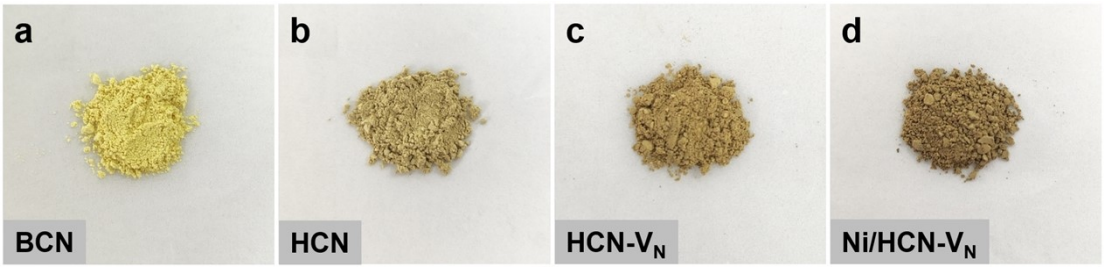


**Fig. S2.** The color of (a) BCN, (b) HCN, (c) HCN-$V_N$ and (d) Ni/HCN-$V_N$.

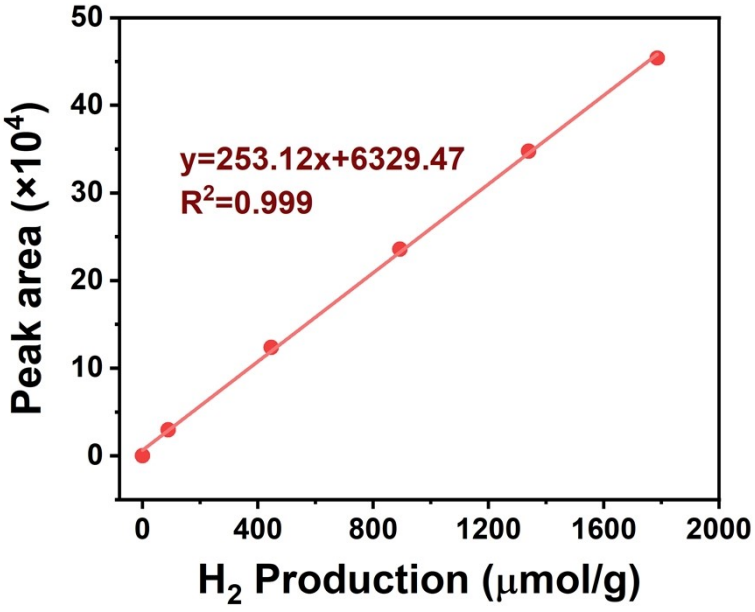


**Fig. S3.** Standard curve for $H_2$ calibration by peak area.

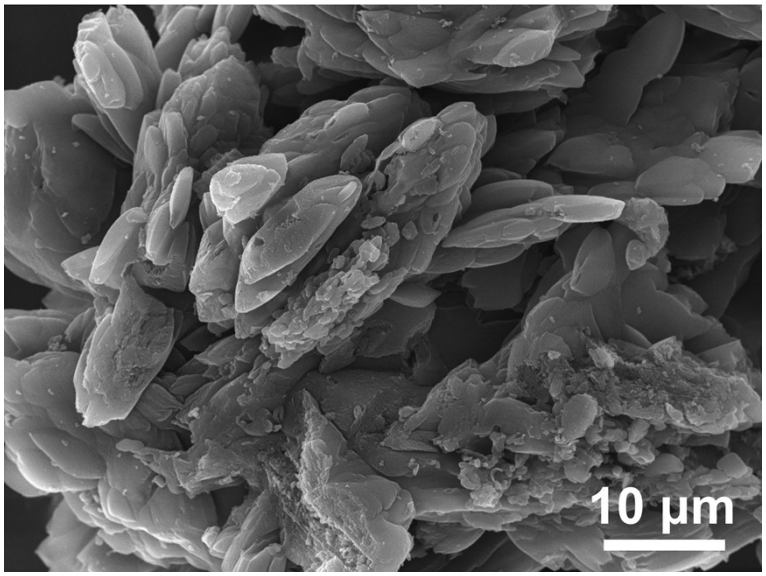


**Fig. S4.** The SEM image of BCN.

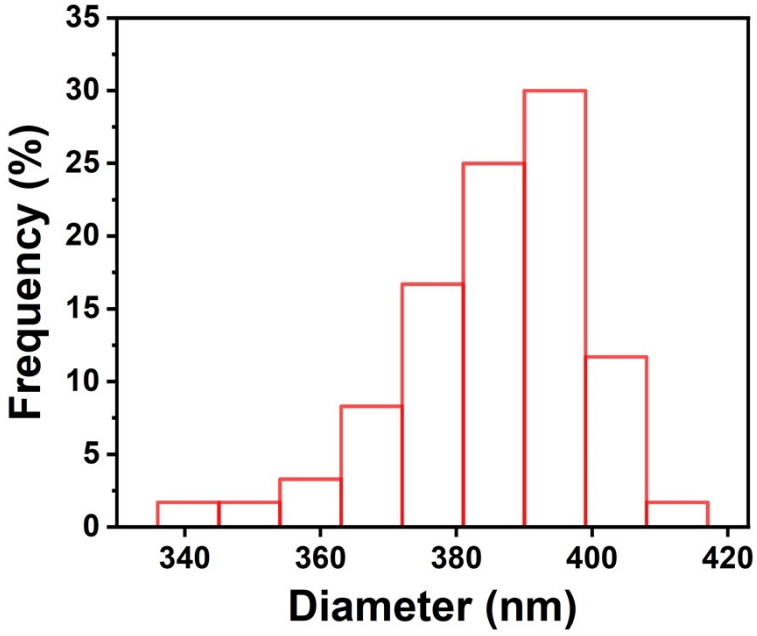


**Fig. S5.** The diameter size distribution of $SiO_2$.

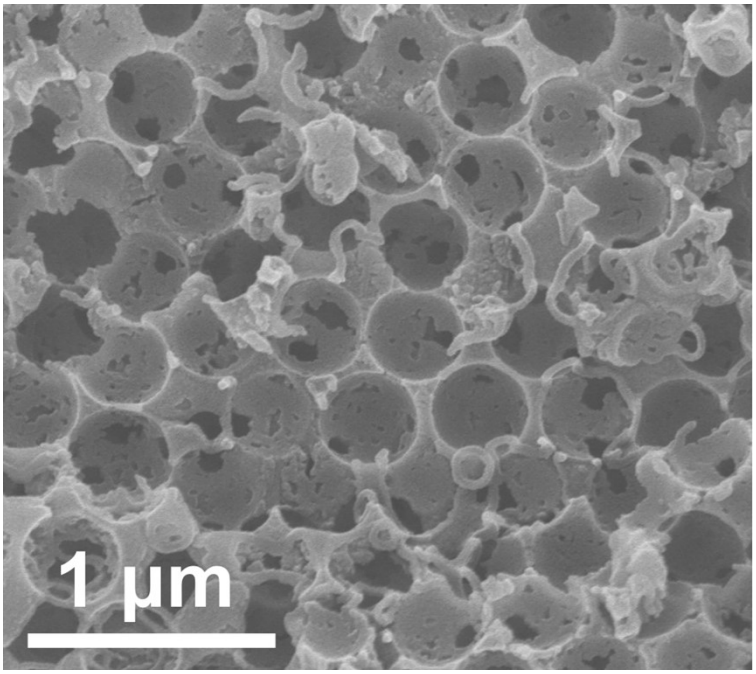


**Fig. S6.** The SEM image of HCN-$V_N$.

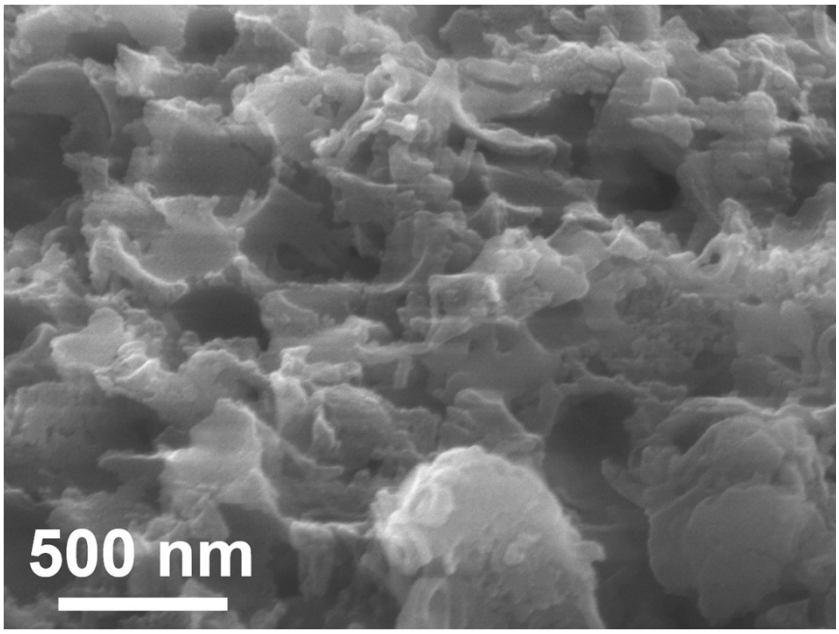


**Fig. S7.** The enlarged SEM image of Ni/HCN-d-$V_N$.

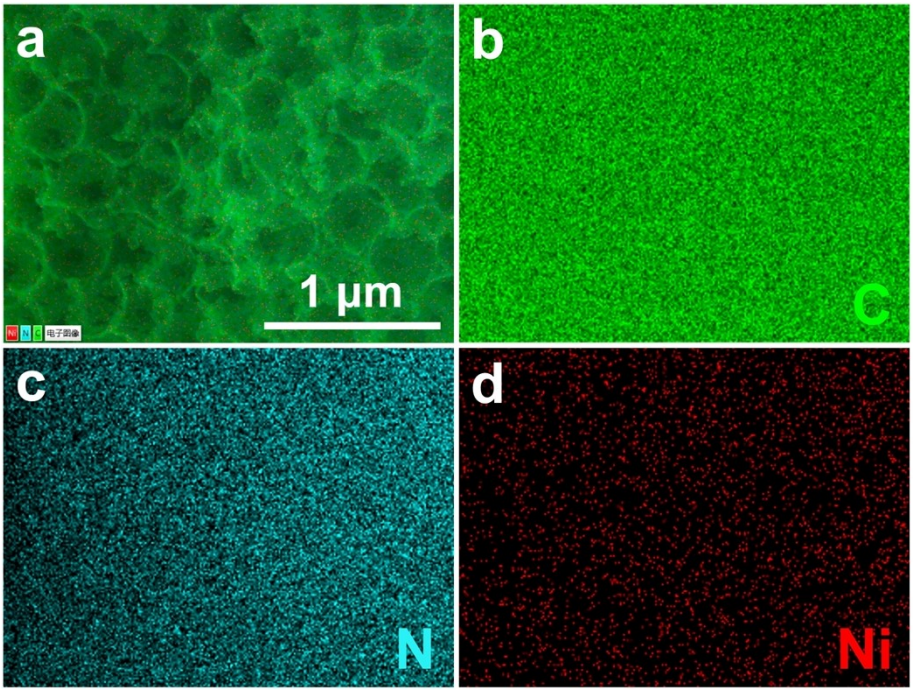


**Fig. S8.** (a) SEM image, (b-d) corresponding EDX elemental mapping profiles of Ni/HCN-$V_N$ with C (green), N (blue), and Pt (red) distribution.

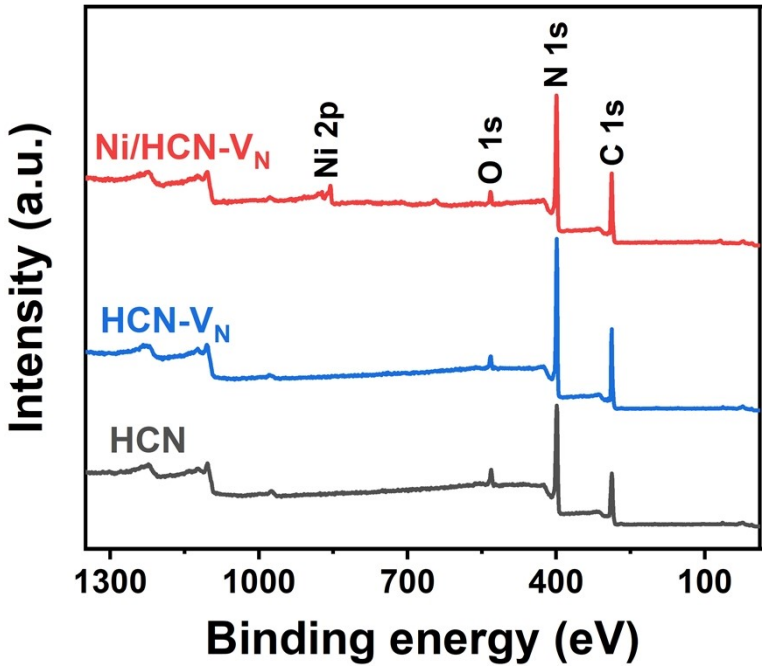


**Fig. S9.** XPS spectra survey of HCN, HCN-$V_N$, and Ni/HCN-$V_N$.

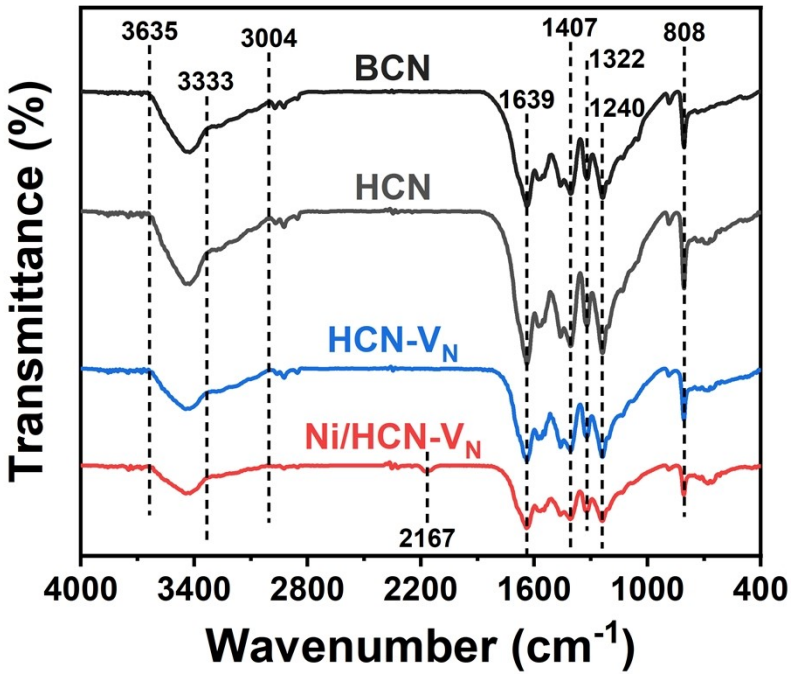


**Fig. S10.** FT-IR spectrum of BCN, HCN, HCN-$V_N$ and Ni/HCN-$V_N$.

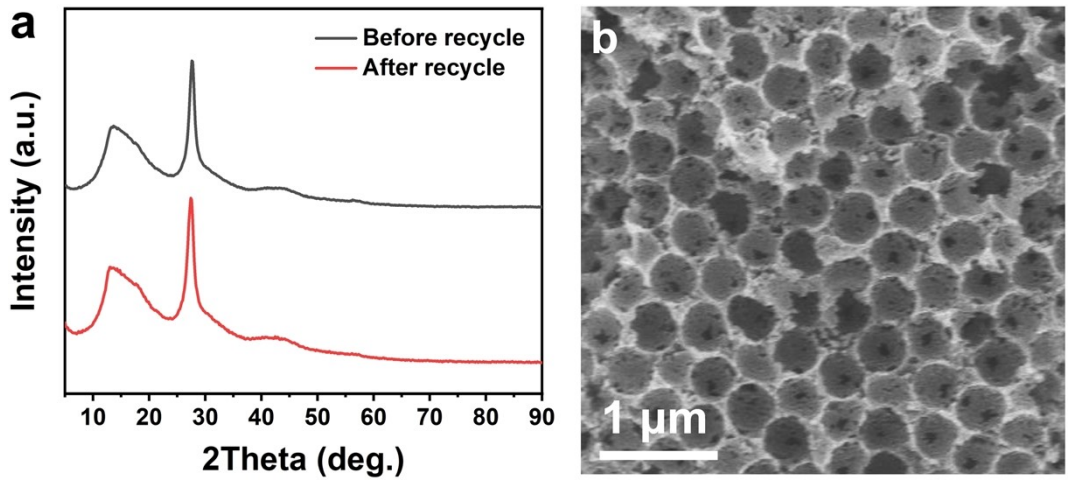


**Fig. S11.** (a) XRD patterns of Ni/HCN-$V_N$ before and after recycling tests and (b) SEM image of Ni/HCN-$V_N$ after recycling tests.

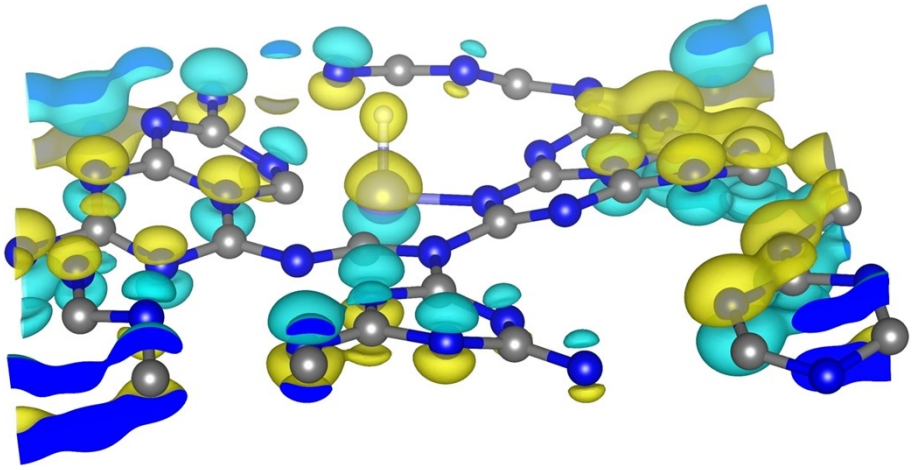

**Fig. S12.** Bader charge density difference for H* adsorption of Ni/HCN-$V_N$.

## S3. Supporting tables

**Table S1.** Photocatalytic $H_2$ production performance comparison of $C_3N_4$-based photocatalyst.

| Photocatalyst | Light source | Reaction system | $H_2$ production rate (μmol $g^{-1}$ $h^{-1}$) | Ref. |
|---|---|---|---|---|
| Pt/NV-CN | 300 W Xe lamp | Methanol (10 vol%) | 323.90 | 6 |
| Eu/g-$C_3N_4$ | 300 W Xe lamp | TEOA (15 vol%) | 128.8 | 7 |
| (P, Mo)-g-$C_3N_4$ | 300 W Xe lamp (λ > 420 nm) | TEOA (5 vol%) | 118 | 8 |
| $Co_3O_4$/g-$C_3N_4$ | 300 W Xe lamp | Triethanolamine (15 vol%) | 105.06 | 9 |
| Pd/NV-CN | 300 W Xe lamp | Methanol (10 vol%) | 287.94 | 10 |
| $MoS_2$/g-$C_3N_4$/NCDs | 300 W Xe lamp (λ > 420 nm) | TEOA (10 vol%) | 212.41 | 11 |
| Pt/$K^+$/cyano group/g-$C_3N_4$ | 300 W Xe lamp (λ > 420 nm) | TEOA (10 vol%) | 332 | 12 |
| g-$C_3N_4$/$WS_2$ | 300 W Xe arc lamp (λ ≥ 420 nm) | Methanol (25 vol%) | 101 | 13 |
| 2D BP/2D $C_3N_4$ | 300 W Xenon lamp (λ > 400 nm) | BPA (10 mg/L) | 259.04 | 14 |
| g-$C_3N_4$/Au/$BiVO_4$ | 300W xenon lamp (λ≥420 nm) | Triethanolamine (20 vol%) | 410.0 | 15 |
| 2D/2D $C_3N_4$/$MoS_2$ | 300W Xenon lamp (λ > 400 nm) | Methyl alcohol (10 vol%) | 385.04 | 16 |
| $Ni(OH)_2$@g-$C_3N_4$/halloysite | 300W Xenon lamp (λ > 400 nm) | $CH_3OH$ (10 vol%) | 122.8 | 17 |
| Pt-PEDOT/$C_3N_4$ | 300 W Xe lamp (λ > 400 nm) | TEOA (10 vol%) | 327 | 18 |
| Pt@Au/g-$C_3N_4$ | 500 W HBO lamp (λ ≥ 420 nm) | TEOA (10 vol%) | 116 | 19 |
| g-$C_3N_4$/Graphene/$MoS_2$ | visible light (λ> 420 nm) | TEOA (0.1 M) | 317 | 20 |
| $MoS_2$/g-$C_3N_4$ | 300 W Xe lamp (λ > 400 nm) | TEOA (10 vol%) | 252 | 21 |
| Au-PtO/g-$C_3N_4$ | 350 W Xe arc lamp (λ > 400 nm) | Methanol (25 vol%) | 338 | 22 |
| Pt/carbon/g-$C_3N_4$ | 350 W Xe lamp (λ ≥ 420 nm) | TEOA (15 vol%) | 212.8 | 23 |
| Pt-CoP/g-$C_3N_4$ | 300 W Xe lamp | Methanol (10 vol%) | 281.25 | 24 |
| Ni/HCN-$V_N$ | 300 W Xe lamp | Methanol (10 vol%) | 420.02 | This work |

**Table S2.** Surface composition of HCN, HCN-$V_N$ and Ni/HCN-$V_N$ as determined by means of XPS.

| | C [wt %] | N [wt %] | Ni [wt %] |
|---|---|---|---|
| HCN | 43.96 | 56.04 | / |
| HCN-$V_N$ | 44.82 | 55.18 | / |
| Ni/HCN-$V_N$ | 45.01 | 53.03 | 1.96 |

## References


1. Q. M. Ahkam, E. U. Khan, J. Iqbal, A. Murtaza and M. T. Khan, Synthesis and characterization of cobalt-doped $SiO_2$ nanoparticles, *Physica B: Condensed Matter*, 2019, **572**, 161-167.
2. G. Kresse and J. Furthmiiller, Efficiency of ab-initio total energy calculations for metals and semiconductors using a plane-wave basis set, *Computational Materials Science*, 1996, **6**, 15-50.
3. G. Kresse and J. Furthmüller, Efficient iterative schemes for ab initio total-energy calculations using a plane-wave basis set, *Physical Review B*, 1996, **54**, 11169-11186.
4. J. P. Perdew, K. Burke and M. Ernzerhof, Generalized Gradient Approximation Made Simple, *Phys. Rev. Lett.*, 1996, **77**, 3865-3868.
5. S. Grimme, J. Antony, S. Ehrlich and H. Krieg, A consistent and accurate ab initio parametrization of density functional dispersion correction (DFT-D) for the 94 elements H-Pu, *J. Chem. Phys.*, 2010, **132**, 154104.
6. Z. H. Zhao, G. M. Ren, Z. S. Zhang, X. C. Meng and Z. Z. Li, Rapid Joule heating synthesis of Pt clusters on $C_3N_4$ with abundant nitrogen vacancies for highly-efficiently photocatalytic $H_2$ production, *Sep. Purif. Technol.*, 2024, **330**, 125393.
7. Y. M. Li, C. X. Lai, J. B. Zhong and J. Z. Li, Largely elevated photocatalytic hydrogen generation over Eu doped g-$C_3N_4$ photocatalyst, *Int. J. Hydrogen Energy*, 2023, **48**, 24356-24368.
8. D. Chen, J. Liu, Z. Jia, J. Fang, F. Yang, Y. Tang, K. Wu, Z. Liu and Z. Fang, Efficient visible-light-driven hydrogen evolution and Cr(VI) reduction over porous P and Mo co-doped g-$C_3N_4$ with feeble N vacancies photocatalyst, *J. Hazard. Mater.*, 2019, **361**, 294-304.
9. Z. D. Xu, J. B. Zhong, J. F. Chen, M. J. Li, L. Zeng and H. Yang, Construction of S-scheme $Co_3O_4$/g-$C_3N_4$ heterojunctions with boosted photocatalytic $H_2$ production performance, *Surfaces and Interfaces*, 2023, **38**, 102838.
10. Y. Yao, G. Ren, Z. Li, H. Bai, X. Hu and X. Meng, Nitrogen Vacancy-Induced Deposition of Pd Nanoparticles onto g-$C_3N_4$ with Greatly Improved Photocatalytic Activity in $H_2$ Evolution, *Solar RRL*, 2021, **5**, 2100145.
11. Y. Jiao, Q. Huang, J. Wang, Z. He and Z. Li, A novel $MoS_2$ quantum dots (QDs) decorated Z-scheme g-$C_3N_4$ nanosheet/N-doped carbon dots heterostructure photocatalyst for photocatalytic hydrogen evolution, *Applied Catalysis B: Environmental*, 2019, **247**, 124-132.
12. J. Yang, Y. Liang, K. Li, G. Yang, K. Wang, R. Xu and X. Xie, Cyano and potassium-rich g-$C_3N_4$ hollow tubes for efficient visible-light-driven hydrogen evolution, *Catalysis Science & Technology*, 2019, **9**, 3342-3346.
13. M. S. Akple, J. Low, S. Wageh, A. A. Al-Ghamdi, J. Yu and J. Zhang, Enhanced visible light photocatalytic $H_2$-production of g-$C_3N_4$/$WS_2$ composite heterostructures, *Appl. Surf. Sci.*, 2015, **358**, 196-203.
14. X. Zhang, J. J. Deng, J. Yan, Y. H. Song, Z. Mo, J. C. Qian, X. Y. Wu, S. Q.

Yuan, H. M. Li and H. Xu, Cryo-mediated liquid-phase exfoliated 2D BP coupled with 2D $C_3N_4$ to photodegradate organic pollutants and simultaneously generate hydrogen, *Appl. Surf. Sci.*, 2019, **490**, 117-123.

15. M. T. Song, Y. H. Wu, G. P. Zheng, C. F. Du and Y. G. Su, Junction of porous g-$C_3N_4$ with $BiVO_4$ using Au as electron shuttle for cocatalyst-free robust photocatalytic hydrogen evolution, *Appl. Surf. Sci.*, 2019, **498**, 143808.
16. W. B. Li, L. Wang, Q. Zhang, Z. Y. Chen, X. Y. Deng, C. Feng, L. K. Xu and M. X. Sun, Fabrication of an ultrathin 2D/2D $C_3N_4/MoS_2$ heterojunction photocatalyst with enhanced photocatalytic performance, *J. Alloys Compd.*, 2019, **808**, 151681.
17. M. Hojamberdiev, M. M. Khan, Z. Kadirova, K. Kawashima, K. Yubuta, K. Teshima, R. Riedel and M. Hasegawa, Synergistic effect of g-$C_3N_4$, $Ni(OH)_2$ and halloysite in nanocomposite photocatalyst on efficient photocatalytic hydrogen generation, *Renewable Energy*, 2019, **138**, 434-444.
18. Z. Xing, Z. Chen, X. Zong and L. Wang, A new type of carbon nitride-based polymer composite for enhanced photocatalytic hydrogen production, *Chem Commun (Camb)*, 2014, **50**, 6762-6764.
19. Y. Di, X. Wang, A. Thomas and M. Antonietti, Making Metal Carbon Nitride Heterojunctions for Improved Photocatalytic Hydrogen Evolution with Visible Light, *ChemCatChem*, 2010, **2**, 834-838.
20. Y.-J. Yuan, Y. Yang, Z. Li, D. Chen, S. Wu, G. Fang, W. Bai, M. Ding, L.-X. Yang, D.-P. Cao, Z.-T. Yu and Z.-G. Zou, Promoting Charge Separation in g-$C_3N_4$/Graphene/$MoS_2$ Photocatalysts by Two-Dimensional Nanojunction for Enhanced Photocatalytic $H_2$ Production, *ACS Applied Energy Materials*, 2018, **1**, 1400-1407.
21. H. Zhao, Y. Dong, P. Jiang, H. Miao, G. Wang and J. Zhang, In situ light-assisted preparation of $MoS_2$ on graphitic $C_3N_4$ nanosheets for enhanced photocatalytic $H_2$ production from water, *Journal of Materials Chemistry A*, 2015, **3**, 7375-7381.
22. J. Jiang, J. Yu and S. Cao, Au/PtO nanoparticle-modified g-$C_3N_4$ for plasmon-enhanced photocatalytic hydrogen evolution under visible light, *J. Colloid Interface Sci.*, 2016, **461**, 56-63.
23. Q. Xu, B. Cheng, J. Yu and G. Liu, Making co-condensed amorphous carbon/g-$C_3N_4$ composites with improved visible-light photocatalytic $H_2$-production performance using Pt as cocatalyst, *Carbon*, 2017, **118**, 241-249.
24. Z. Pan, Y. Zheng, F. Guo, P. Niu and X. Wang, Decorating CoP and Pt Nanoparticles on Graphitic Carbon Nitride Nanosheets to Promote Overall Water Splitting by Conjugated Polymers, *ChemSusChem*, 2017, **10**, 87-90.